Global Biogeochemical Cycles

Supporting Information for

An assessment of CO_2 storage and sea-air fluxes for the Atlantic Ocean and Mediterranean Sea between 1985 and 2018.

Fiz F. Pérez[1], M. Becker[2], N. Goris[3], M. Gehlen[4], M. López-Mozos[1], J. Tjiputra[3], A. Olsen[2], J.D. Müller[5], I. E. Huertas[6], T. T. T. Chau[4], V. Cainzos[7], A. Velo[1], G. Benard[4], J. Hauck[8], N. Gruber[5] and Rik Wanninkhof[9].

[1]Instituto de Investigaciones Marinas (IIM), CSIC, Vigo, Spain

[2]Geophysical Institute, University of Bergen, and Bjerknes Centre for Climate Research, Bergen, Norway

[3]NORCE Climate & Environment, Bjerknes Centre for Climate Research, Bergen, Norway

[4]Laboratoire des Sciences du Climat et de l'Environnement, LSCE/IPSL, CEA-CNRS-UVSQ, Université, Paris-Saclay, F-91191 Gif-sur-Yvette, France

[5]Environmental Physics, Institute of Biogeochemistry and Pollutant Dynamics, ETH Zurich, Zürich, Switzerland

[6]Instituto de Ciencias Marinas de Andalucía (ICMAN-CSIC), Puerto Real, Cadiz, Spain

[7]Unidad Océano y Clima, Instituto de Oceanografía y Cambio Global, IOCAG, Universidad de Las Palmas de Gran Canaria, ULPGC, Unidad Asociada ULPGC-CSIC, Canary Islands, Spain

[8]Alfred-Wegener-Institut, Helmholtz-Zentrum für Polar- und Meeresforschung, Bremerhaven, Germany

[9]Atlantic Oceanographic and Meteorological Laboratory, National Oceanic and Atmospheric Administration, Miami, Florida, USA

Corresponding authors: Fiz F. Pérez (fiz.perez@iim.csic.es) and M. López-Mozos (mlopezm@iim.csic.es)

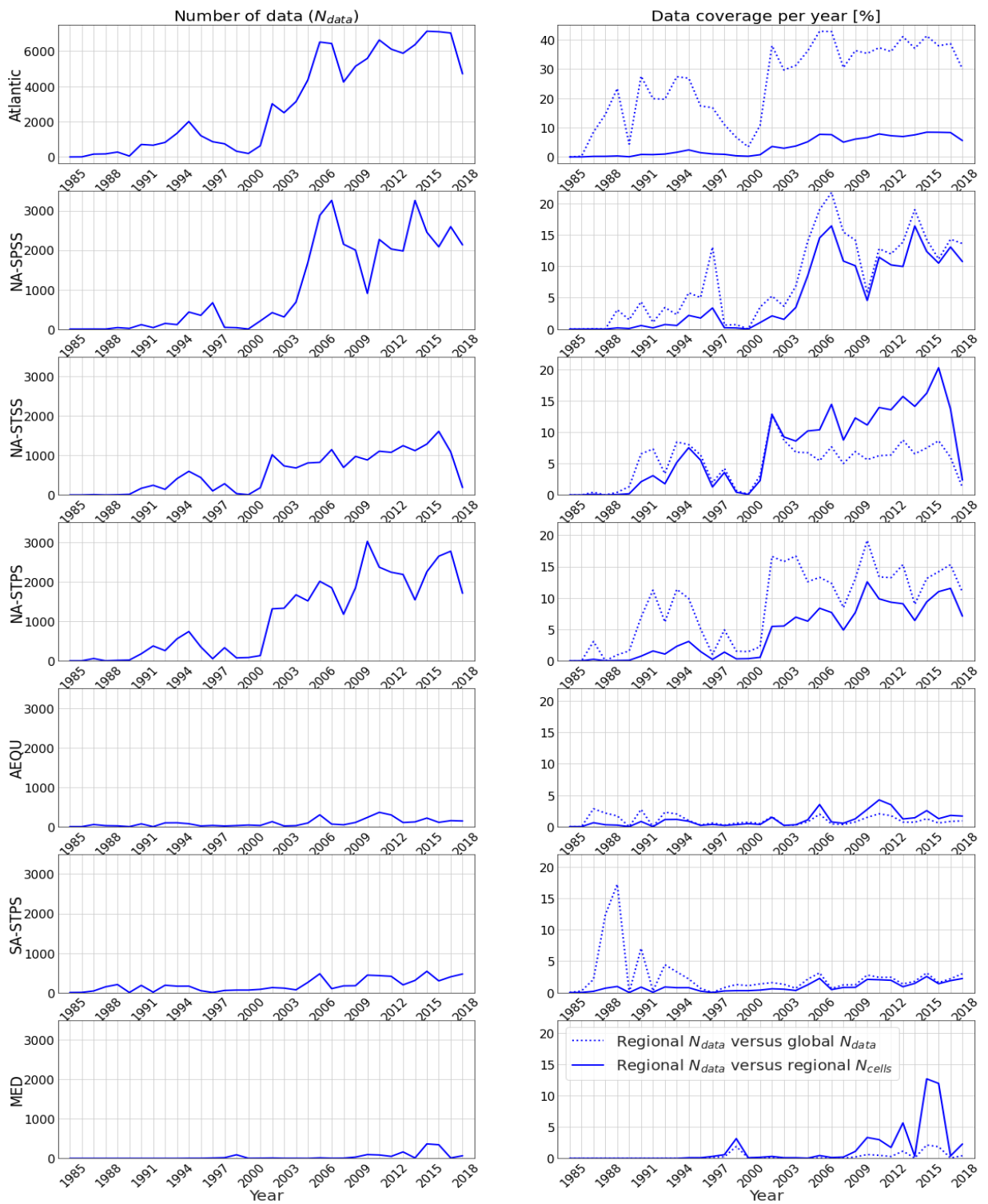

Supplementary Figure S1. Number of pixels with observations in SOCAT2020 for the Atlantic Ocean and all its biomes (Left). Right panels show data coverage (%) in relation to the total pixels with SOCAT data over the global ocean for each year (dotted line) and in relation to the maximum pixel in each biome multiplied by 12 (plain line).

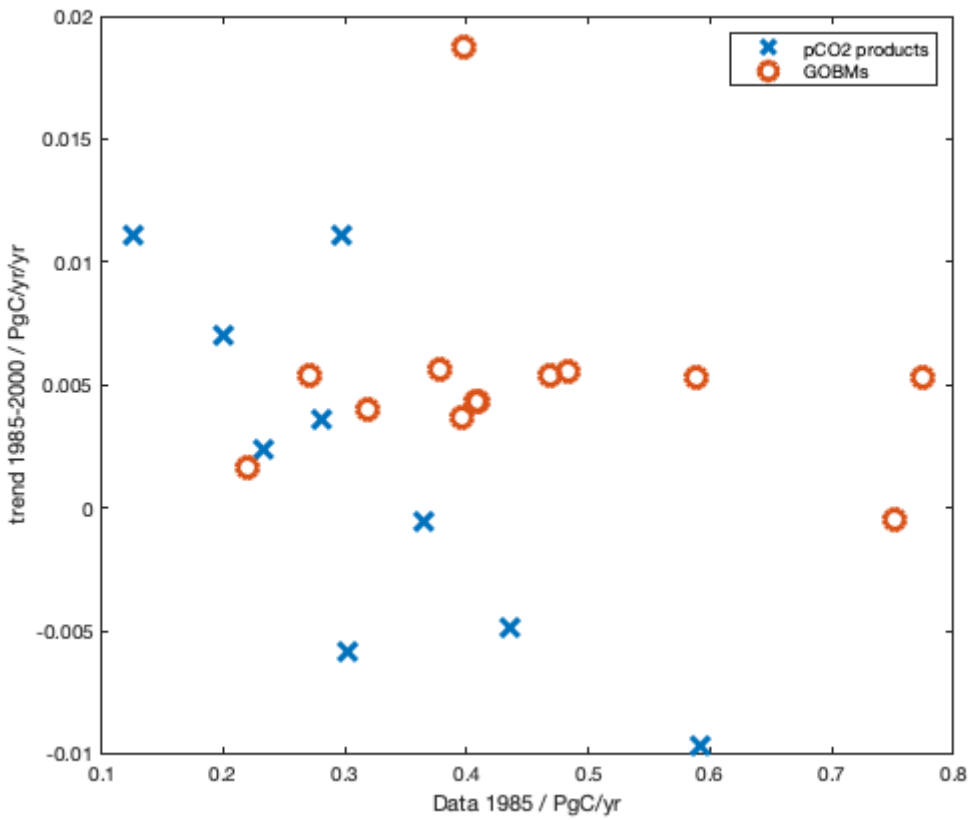

Supplementary Figure S2. Trends of FCO_2 between 1985 and 2000 versus the FCO_2 in 1985. GOBMs do not show any correlation (red circles). pCO_2 products in blue crosses show that products with high FCO_2 in 1985 tend to have high negative trends along the period 1985-2000.

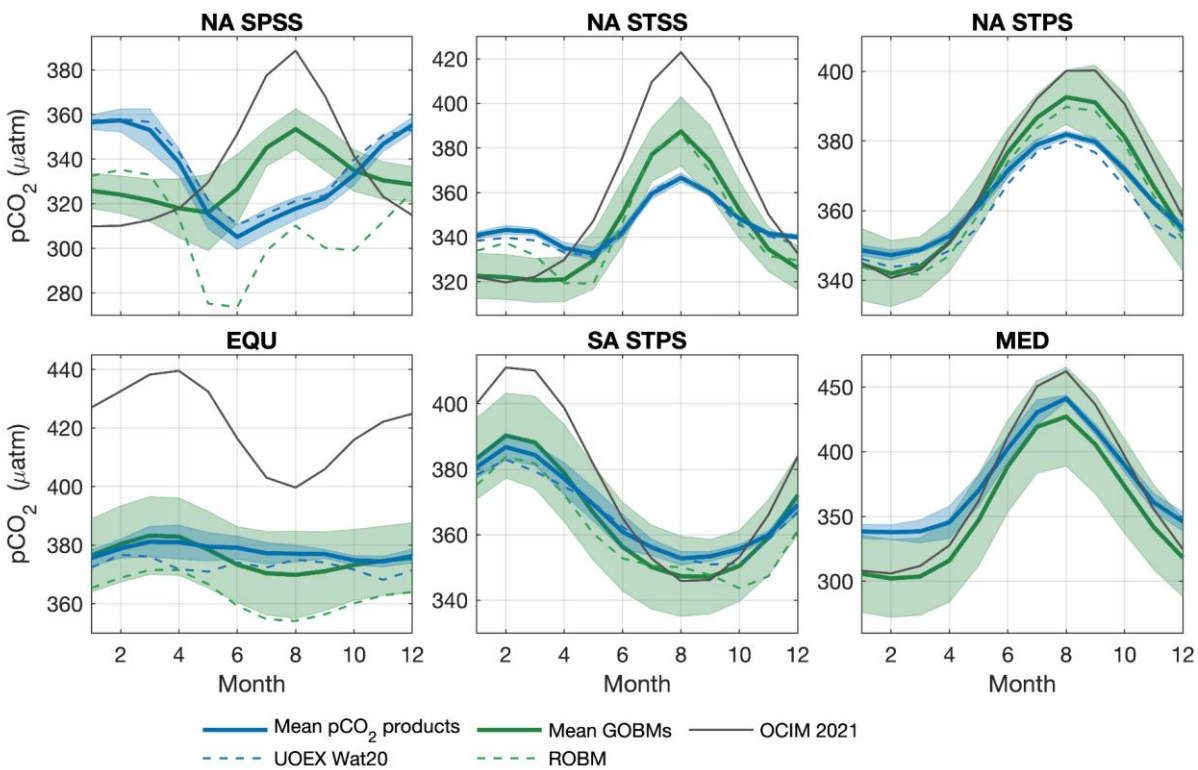

Supplementary Figure S3. Seasonal cycle of the pCO_2 for each Atlantic biome as estimated by pCO_2 products (blue) and GOBMs (green), both shown as the ensemble mean (thick lines) and 1σ spread (ribbons). Additional lines represent UOEX, OCIM and one ROBM.

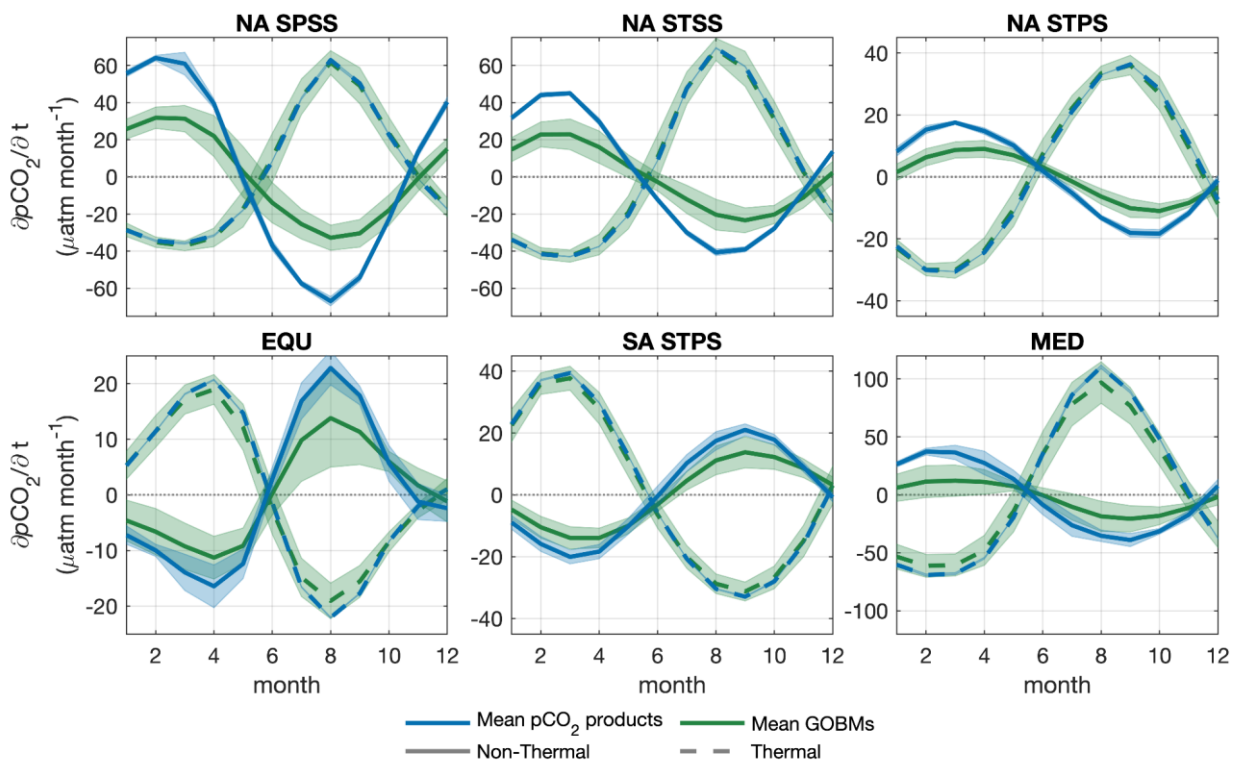

Supplementary Figure S4. Seasonal cycle of the rate of change of the thermal (color broken lines) and non-thermal components (color lines) of ocean surface pCO_2 on monthly time scales given µatm month^{-1} for each Atlantic biome as estimated by pCO_2 products (blue) and GOBMs (green), both shown as the ensemble mean (thick lines) and 1σ spread (ribbons).

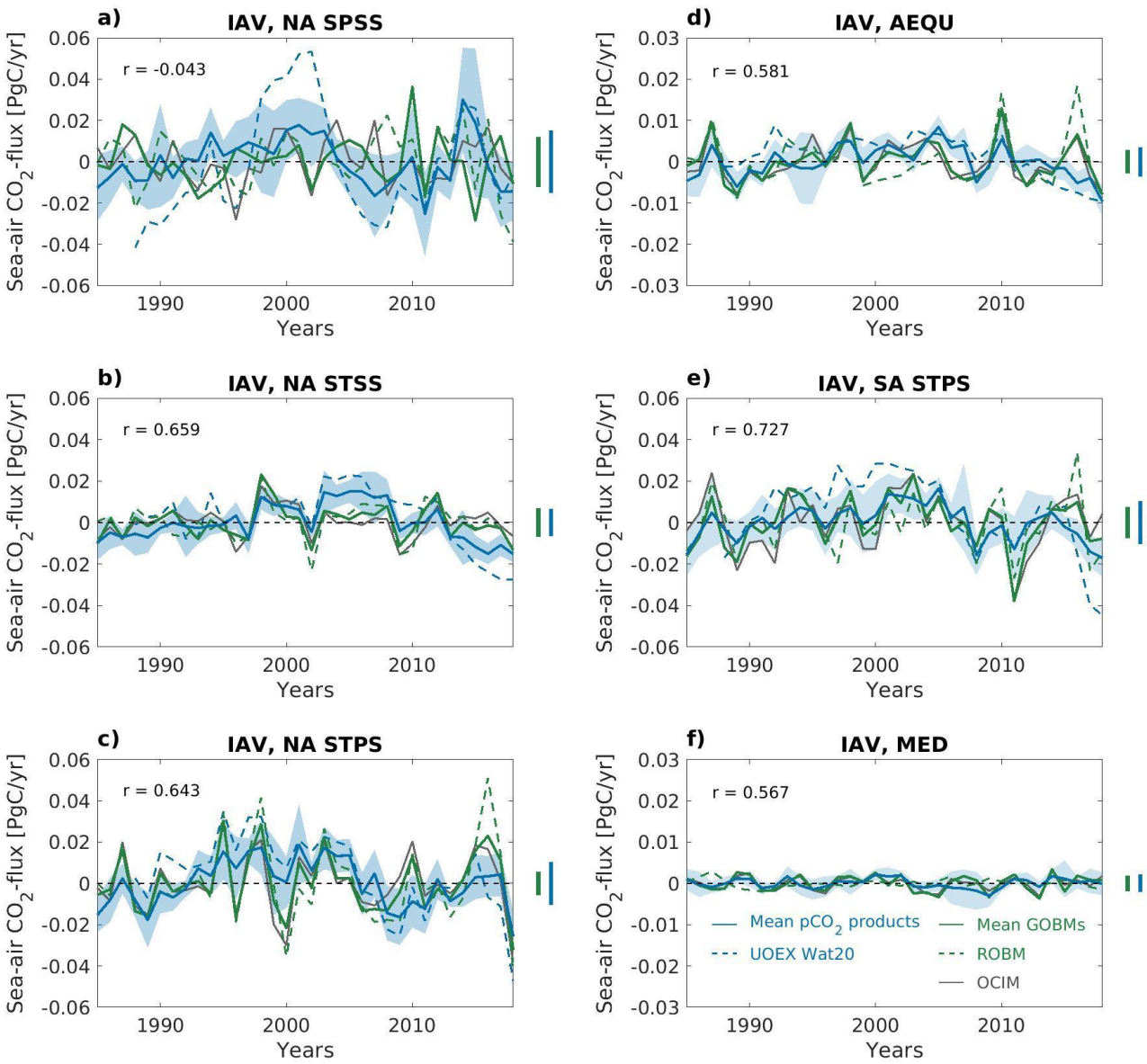

Supplementary Figure S5. Time-series of detrended annual air-sea CO_2 flux anomalies visualizing the Interannual Variability (IAV) for all Atlantic biomes. Illustrated are both GOBMs (mean: green line; std: green shading) and pCO_2 products (mean: blue line; std: blue shading), as well as the correlation between the time-series of GOBMs and pCO_2 products (denoted in the upper left corner of each panel) and the IAV amplitude for both GOBMs and pCO_2 products (illustrated as colored lines on the right side of each plot).

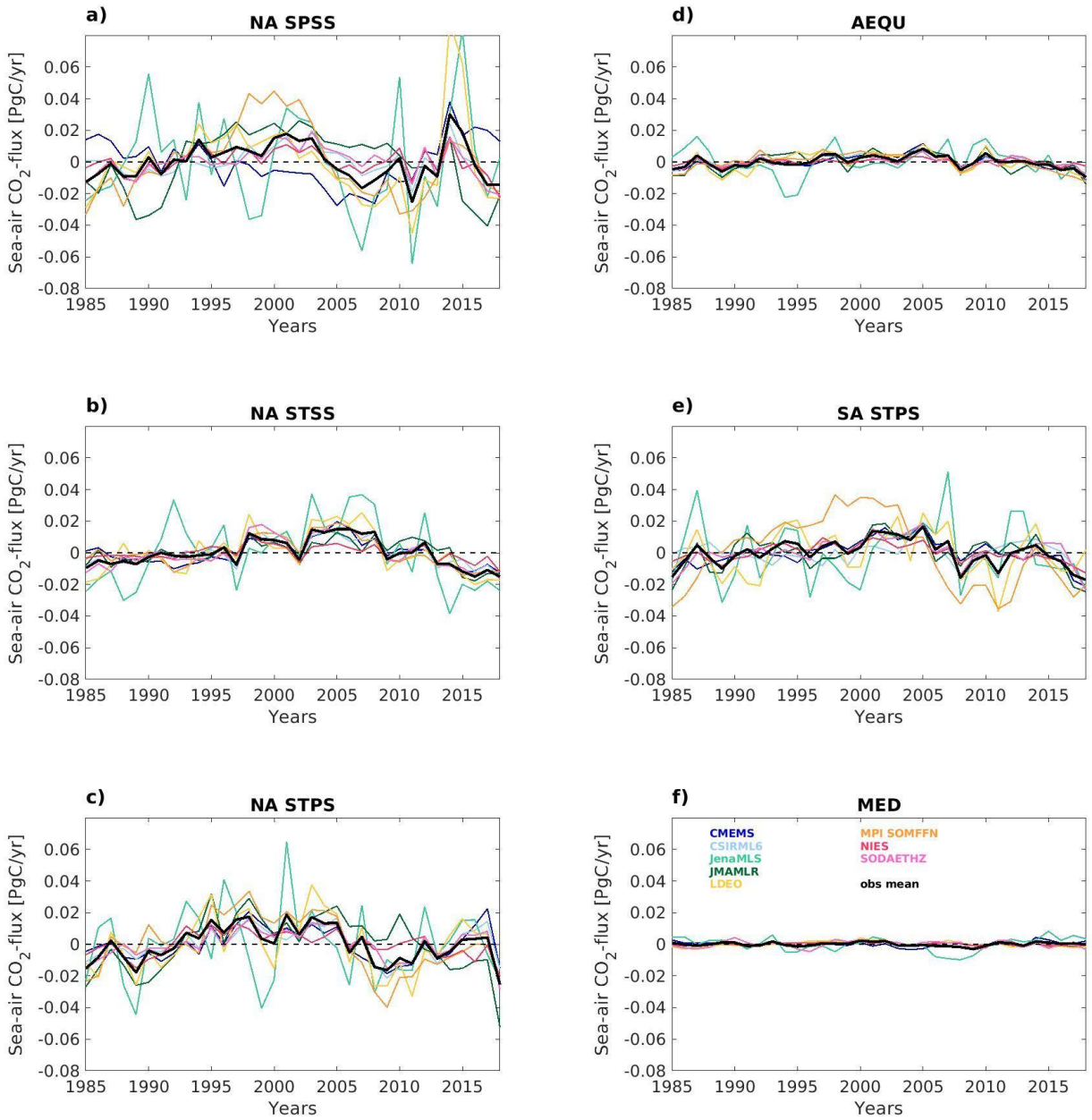

Supplementary Figure S6. Time-series of detrended annual air-sea CO_2 flux anomalies visualizing the Interannual Variability (IAV) for all Atlantic biomes. Illustrated are results for the individual pCO_2 products (coloured lines) and the ensemble mean for all pCO_2 products (black line).

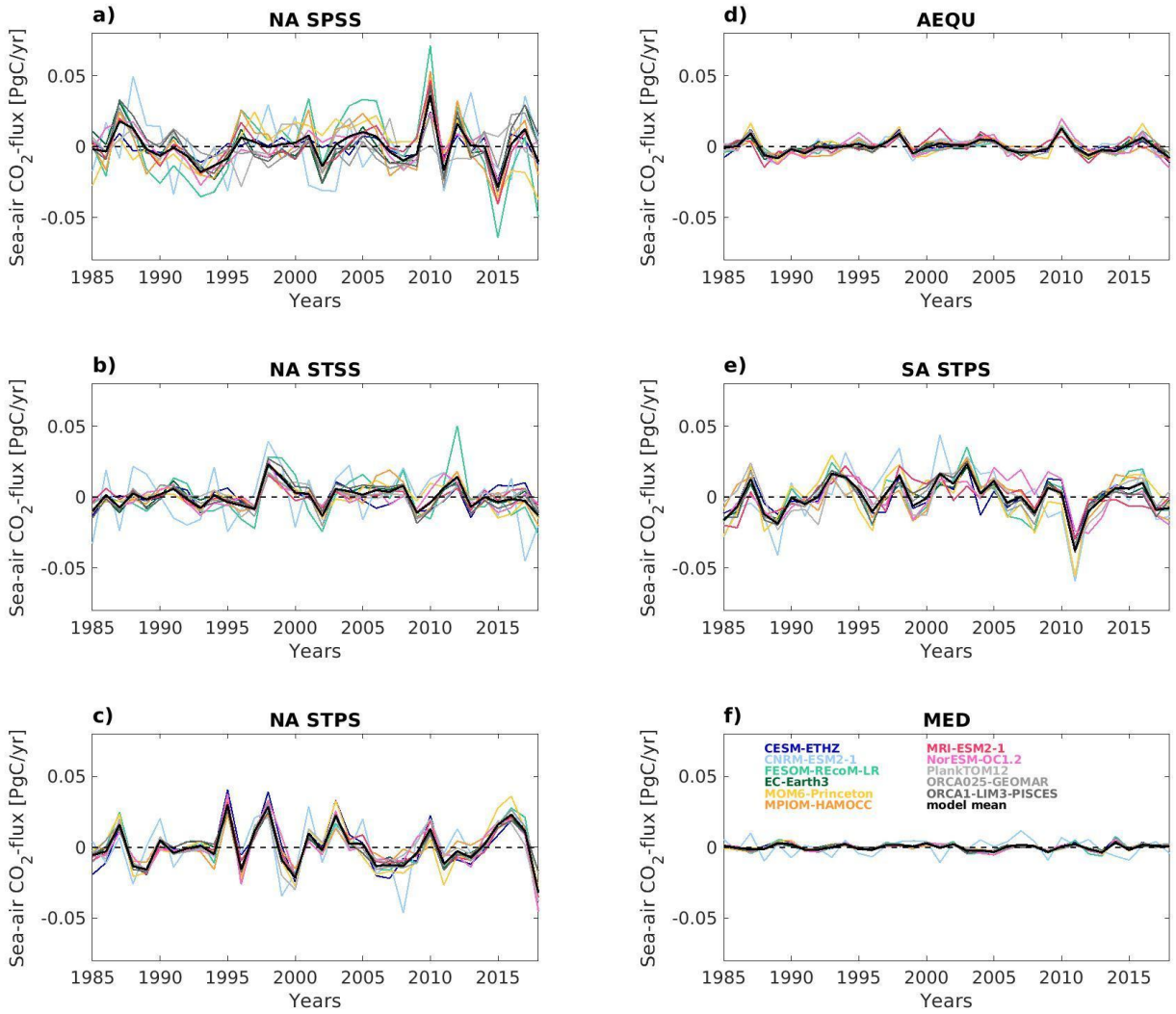

Supplementary Figure S7. Time-series of detrended annual air-sea CO_2 flux anomalies visualizing the Interannual Variability (IAV) for all Atlantic biomes. Illustrated are results for the individual GOBMs (coloured lines) and the ensemble mean for all GOBMs (black line).

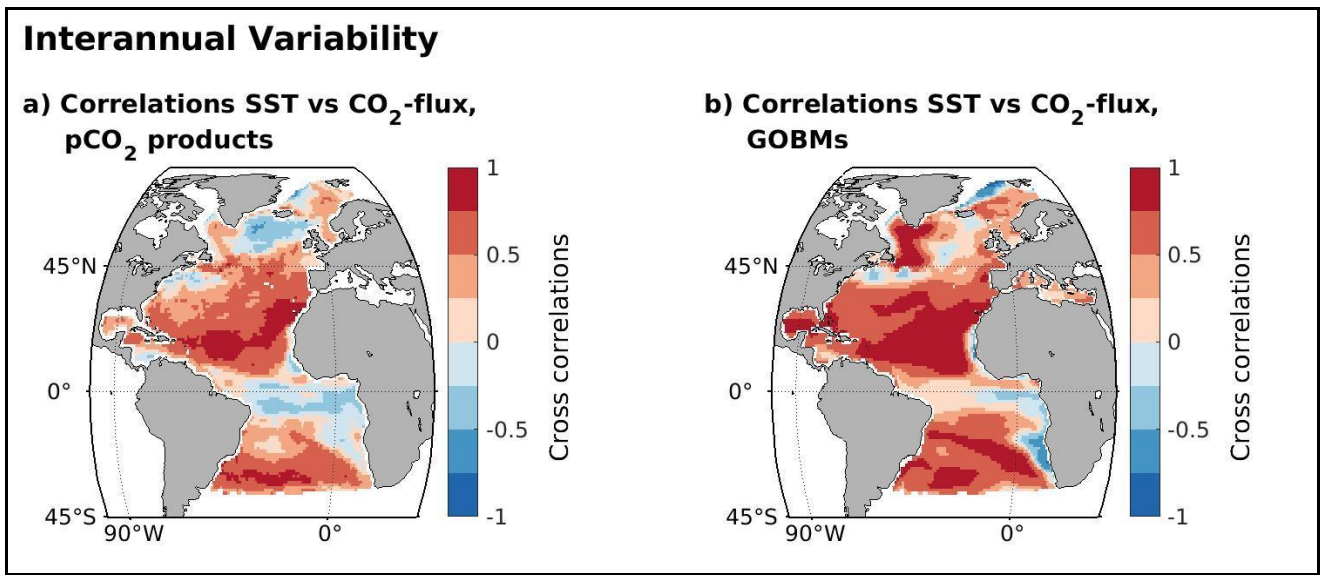

Supplementary Figure S8. Cross-correlation between the ensemble-averaged time-series of detrended annual air-sea CO_2 flux anomalies and the ensemble-averaged time-series of detrended annual SST anomalies for (a) pCO_2 products (note that only 5 pCO_2 products provided SST-data) and (b) GOBMs.

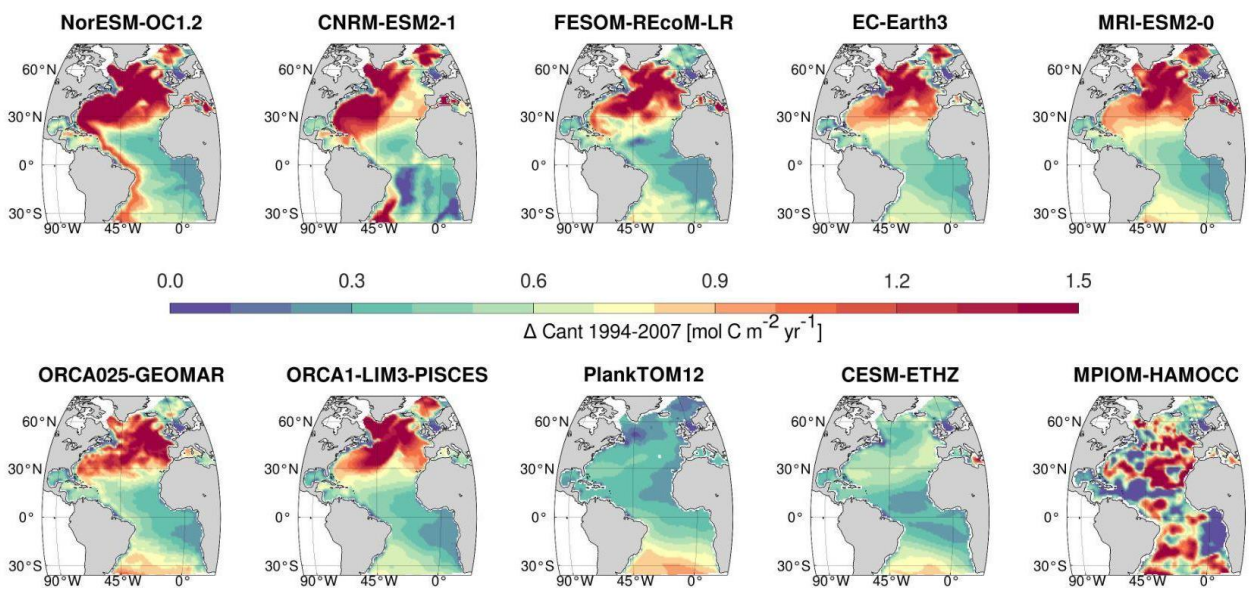

Supplementary Figure S9. Column inventories of anthropogenic carbon storage rates (1994-2007), integrated from surface to 3000m, of each individual GOBM in the Atlantic.

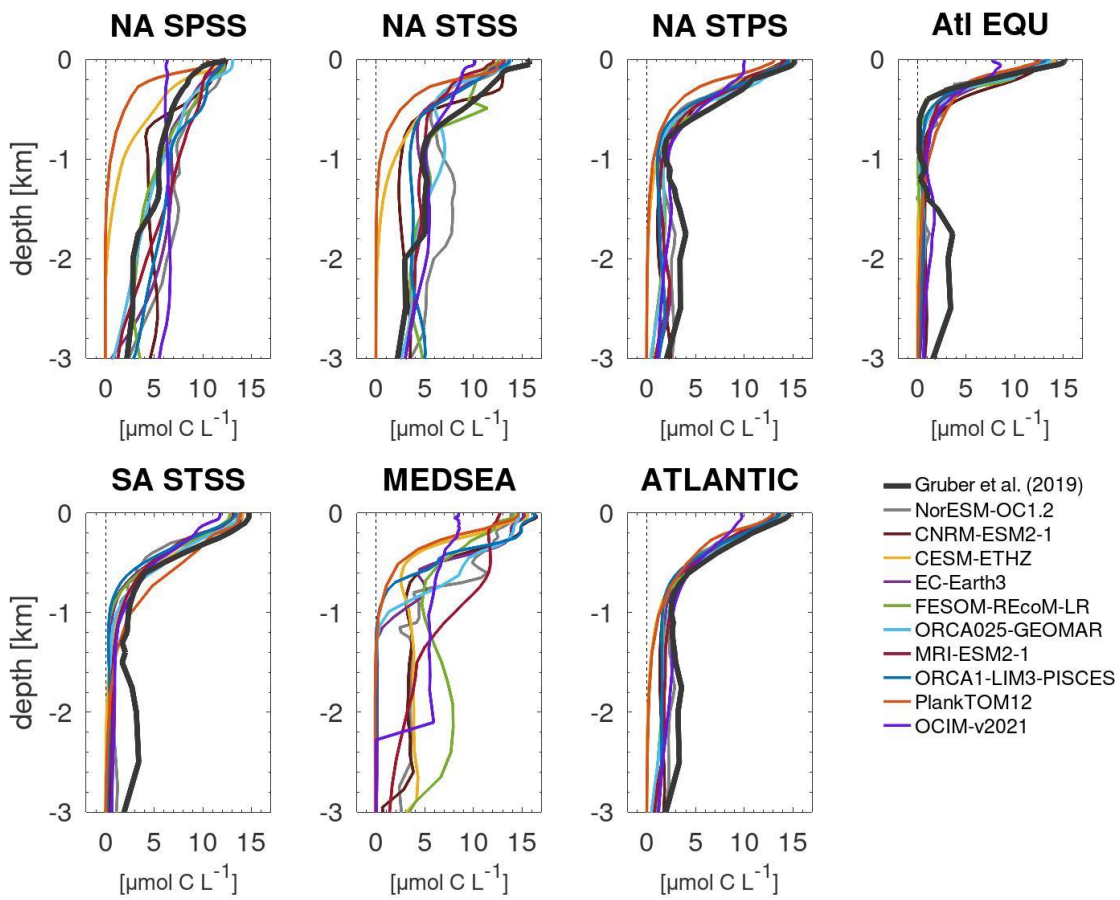

Supplementary Figure S10. Average vertical profiles of ΔC_{ant} (1994-2007; Sim_A – Sim_D) of each GOBM for all Atlantic biomes. OCIM-v2021 values depict differences in DIC concentration between 2007 and 1994 in Sim_A. Black lines represent observational-based ΔC_{ant}, using the eMLR(ΔC*) from Gruber et al., (2019). Note that there is no observational-based estimate for the Mediterranean Sea. The ATLANTIC panel includes all biomes except the MED.

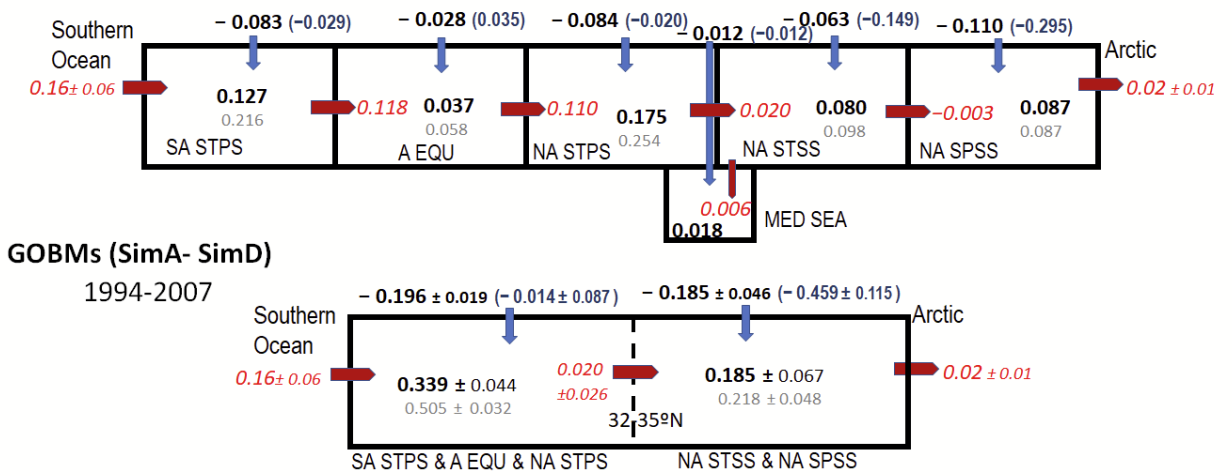

Supplementary Figure S11. Average of anthropogenic CO_2 budget (Pg C yr^{-1}) in the Atlantic from GOBMs using Sim_A- sim_D from 1994 to 2007. *Blue arrows indicate sea-air CO_2 fluxes and red arrows indicate lateral transport of C_{ant}* at the boundaries of the different biomes. C_{ant} storage and air-sea C_{ant} flux are given in black bold numbers. Total air-sea FCO_2 fluxes (Fig 1) are given between parentheses in blue. Red numbers are northward advection of C_{ant} transport inferred by difference between C_{ant} storage rate and air-sea uptake.

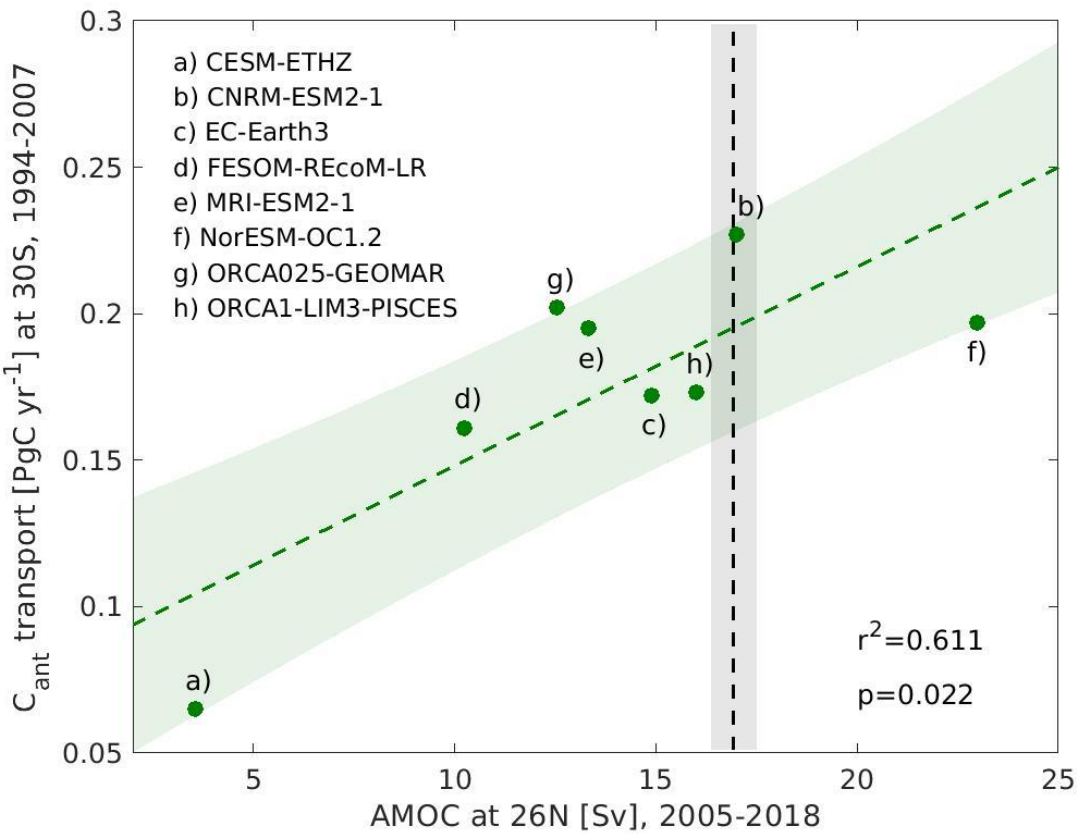

Supplementary Figure S12. C_{ant} transport at 30ºS versus AMOC at 26ºN. Anthropogenic carbon transport at 30ºS averaged from 1994 to 2007 plotted against the Atlantic Meridional Overturning Circulation at 26°N averaged from 2005 to 2018. Illustrated are linear fits (green dashed line) with 68% projection intervals (green shaded area) across GOBMs (green dots). The observation-based estimate of the AMOC and its uncertainty are marked with dashed black lines and black shaded areas. Here, data from the RAPID-Meridional Overturning Circulation and Heatflux Array-Western Boundary Time Series array at 26°N were used (Frajka-Williams et al., 2021).